Improvement of Ship Motion Control Using a Magnitude-Rate Saturation Model

Ole Nikolai Lyngstadaas, Tore Egil Sæterdal, Mikkel Eske Nørgaard Sørensen, Morten Breivik

***Abstract*— Motion control concepts for ships have traditionally not focused on handling actuator constraints. This paper investigates the effects on performance of a pair of nonlinear control schemes by developing and implementing a magnitude-rate saturation (MRS) model. The effects of using the MRS model is tested in experiments with a model ship in an ocean basin. Performance metrics are used to evaluate performance in terms of control error, energy efficiency, and actuator wear and tear.**

***Index Terms*— Ship motion control, Magnitude-rate saturation model, Constraint handling, Nonlinear control, Model-scale experiments, Wear and tear**

I. INTRODUCTION

In traditional control theory, an ideal controller might achieve perfect reference tracking in simulations, having no or non-sufficient limitations on the control input. However, in real-life applications it would not be feasible due to limitations in physical output and wear and tear of the actuators.

Several ways of handling actuator constraints have been investigated throughout the years. In [1], model predictive control for systems with actuator magnitude and rate constraints is presented. A solution using a modified dynamic window approach to handle actuator constraints is investigated in [2], and further expanded in [3].

To easily include magnitude and rate saturation (MRS) effects into a control system, a possible low-level approach is to limit the output of the control signal within the limits of the actuators. However, this may lead to an under-damped closed-loop system. To avoid this, effort has been put into implementing a model for combining MRS to smoothen the control output within allowed actuator limits. In [4], an MRS model is derived to address the issue of anti-windup, and the MRS model used in this paper is based on this approach.

In particular, the magnitude and rate saturations in this paper are set at lower limits than the actual actuator constraints. The main purpose is to investigate how limiting the actuator's magnitude and rate outputs will impact the overall performance of the motion control system. The MRS model, depending on how it is tuned, can be implemented in a simulation scenario, where the purpose is to mimic the actual constraints of the system, or be used to limit actuator outputs in laboratory experiments and on-board actual vessels.

O. N. Lyngstadaas and T. E. Sæterdal are M.Sc. students at the Department of Engineering Cybernetics, Norwegian University of Science and Technology (NTNU), NO-7491 Trondheim, Norway. M. E. N. Sørensen and M. Breivik are with the Centre for Autonomous Marine Operations and Systems, Department of Engineering Cybernetics, Norwegian University of Science and Technology (NTNU), NO-7491 Trondheim, Norway. Email: {mikkel.e.n.sorensen, morten.breivik}@ieee.org

The main contribution of this paper are the experimental results from scale testing on a 1:90 ship model. The MRS model from [4] is adapted to a three degrees of freedom (DOF) ship model and experimentally tested at the Marine Cybernetics Laboratory (MC-Lab) at the Norwegian University of Science and Technology (NTNU) in Trondheim, Norway. Furthermore, the positive effects of employing MRS to a pair of nonlinear feedback control schemes from [5] have been investigated.

The rest of this paper is organized as follows: Section II presents a mathematical ship model; Section III defines the control objective and the 4-corner test, derivation of the MRS model, and also presents a pair of nonlinear controllers from [5]; Section IV presents the experimental results from model-scale testing in the MC-Lab, while Section V concludes the paper.

II. SHIP MODEL

The motion of a ship can be represented by the pose vector $\boldsymbol{\eta} = [x, y, \psi]^\top \in \mathbb{R}^2 \times \mathbb{S}$ and the velocity vector $\boldsymbol{\nu} = [u, v, r]^\top \in \mathbb{R}^3$. Here, (x, y) represents the Cartesian position in the local earth-fixed reference frame, ψ is the yaw angle, (u, v) represents the body-fixed linear velocities and r is the yaw rate. The 3-DOF dynamics of a ship can then be stated as in [6]:

$$\dot{\boldsymbol{\eta}} = \boldsymbol{R}(\psi)\boldsymbol{\nu} \tag{1}$$

$$\boldsymbol{M}\dot{\boldsymbol{\nu}} + \boldsymbol{C}(\boldsymbol{\nu})\boldsymbol{\nu} + \boldsymbol{D}(\boldsymbol{\nu})\boldsymbol{\nu} = \boldsymbol{\tau}, \tag{2}$$

where $\boldsymbol{M} \in \mathbb{R}^{3\times3}$, $\boldsymbol{C}(\boldsymbol{\nu}) \in \mathbb{R}^{3\times3}$, $\boldsymbol{D}(\boldsymbol{\nu}) \in \mathbb{R}^{3\times3}$ and $\boldsymbol{\tau} = [\tau_1, \tau_2, \tau_3]^\top$ represent the inertia matrix, Coriolis and centripetal matrix, damping matrix and control input vector, respectively. The rotation matrix $\boldsymbol{R}(\psi) \in SO(3)$ is given by

$$\boldsymbol{R}(\psi) = \begin{bmatrix} \cos(\psi) & -\sin(\psi) & 0 \\ \sin(\psi) & \cos(\psi) & 0 \\ 0 & 0 & 1 \end{bmatrix}. \tag{3}$$

The system matrices are assumed to satisfy the properties $\boldsymbol{M} = \boldsymbol{M}^\top > 0$, $\boldsymbol{C}(\boldsymbol{\nu}) = -\boldsymbol{C}(\boldsymbol{\nu})^\top$ and $\boldsymbol{D}(\boldsymbol{\nu}) > 0$.

A. Nominal model

The model and parameters of the model-scale ship C/S Inocean Cat I Drillship (CSAD) [7], as shown in Fig. 1, will be used in this paper. CSAD is a 1:90 scale replica of a supply ship, with a length of $L = 2.578$ m. The inertia matrix is given as

$$\boldsymbol{M} = \boldsymbol{M}_{RB} + \boldsymbol{M}_A, \tag{4}$$

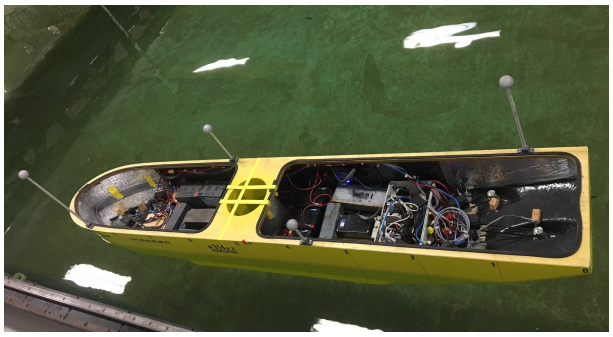

Fig. 1: C/S Inocean Cat I Drillship in the MC-lab.

where

$$\boldsymbol{M}_{RB} = \begin{bmatrix} m & 0 & 0 \\ 0 & m & mx_g \\ 0 & mx_g & I_z \end{bmatrix} \tag{5}$$

$$\boldsymbol{M}_{A} = \begin{bmatrix} -X_{\dot{u}} & 0 & 0 \\ 0 & -Y_{\dot{v}} & -Y_{\dot{r}} \\ 0 & -N_{\dot{v}} & -N_{\dot{r}} \end{bmatrix}. \tag{6}$$

The mass of CSAD is $m = 127.92$ kg, while $x_g = 0.00375$ m is the distance along the x-axis in the body frame from the centre of gravity, and $I_z = 61.987\ \mathrm{kg\,m^2}$ is the moment of inertia about the z-axis in the body frame. Other parameter values are listed in Table I, which are updated values from [7], where a few changes to the numerical values and signs have been done to better fit the actual laboratory performance of CSAD.

CSAD has six azimuth thrusters, which in the experiments presented here are fixed to the angles $\boldsymbol{\delta} = [\pi, \pi/4, -\pi/4, 0, 5\pi/4, 3\pi/4]^\top$ rad, in the body-fixed coordinate system, giving a fully actuated vessel [3].

The Coriolis and centripetal matrix is

$$\boldsymbol{C}(\boldsymbol{\nu}) = \boldsymbol{C}_{RB}(\boldsymbol{\nu}) + \boldsymbol{C}_{A}(\boldsymbol{\nu}), \tag{7}$$

with

$$\boldsymbol{C}_{RB}(\boldsymbol{\nu}) = \begin{bmatrix} 0 & 0 & -m(x_g r + v) \\ 0 & 0 & mu \\ m(x_g r + v) & -mu & 0 \end{bmatrix} \tag{8}$$

$$\boldsymbol{C}_{A}(\boldsymbol{\nu}) = \begin{bmatrix} 0 & 0 & -c_{A,13}(\boldsymbol{\nu}) \\ 0 & 0 & c_{A,23}(\boldsymbol{\nu}) \\ c_{A,13}(\boldsymbol{\nu}) & -c_{A,23}(\boldsymbol{\nu}) & 0 \end{bmatrix}, \tag{9}$$

where

$$c_{A,13}(\boldsymbol{\nu}) = -Y_{\dot{r}} r - Y_{\dot{v}} v \tag{10}$$

$$c_{A,23}(\boldsymbol{\nu}) = -X_{\dot{u}} u. \tag{11}$$

Finally, the damping matrix $\boldsymbol{D}(\boldsymbol{\nu})$ is given as

$$\boldsymbol{D}(\boldsymbol{\nu}) = \boldsymbol{D}_{L} + \boldsymbol{D}_{NL}(\boldsymbol{\nu}), \tag{12}$$

where

$$\boldsymbol{D}_{L} = \begin{bmatrix} -X_u & 0 & 0 \\ 0 & -Y_v & -Y_r \\ 0 & -N_v & -N_r \end{bmatrix} \tag{13}$$

TABLE I: Parameters for CSAD, updated from [7].

Parameter	Value	Parameter	Value
$X_{\dot{u}}$	-3.262	$Y_{\lvert r\rvert r}$	-3.450
$Y_{\dot{v}}$	-28.890	Y_{rrr}	0
$Y_{\dot{r}}$	-0.525	N_r	-6.916
$N_{\dot{v}}$	-0.157	$N_{\lvert r\rvert r}$	-4.734
$N_{\dot{r}}$	-13.980	N_{rrr}	-0.147
X_u	-2.332	N_v	0
$X_{\lvert u\rvert u}$	0	$N_{\lvert v\rvert v}$	-0.209
X_{uuu}	-8.557	N_{vvv}	0
Y_v	-4.673	$N_{\lvert r\rvert v}$	0.080
$Y_{\lvert v\rvert v}$	-0.398	$N_{\lvert v\rvert r}$	0.080
Y_{vvv}	-313.300	$Y_{\lvert r\rvert v}$	-0.805
Y_r	-7.250	$Y_{\lvert v\rvert r}$	-0.845

$$\boldsymbol{D}_{NL}(\boldsymbol{\nu}) = \begin{bmatrix} d_{NL,11}(\boldsymbol{\nu}) & 0 & 0 \\ 0 & d_{NL,22}(\boldsymbol{\nu}) & d_{NL,23}(\boldsymbol{\nu}) \\ 0 & d_{NL,32}(\boldsymbol{\nu}) & d_{NL,33}(\boldsymbol{\nu}) \end{bmatrix}, \tag{14}$$

with

$$d_{NL,11}(\boldsymbol{\nu}) = -X_{|u|u}|u| - X_{uuu}u^2 \tag{15}$$

$$d_{NL,22}(\boldsymbol{\nu}) = -Y_{|v|v}|v| - Y_{|r|v}|v| - Y_{vvv}v^2 \tag{16}$$

$$d_{NL,23}(\boldsymbol{\nu}) = -Y_{|r|r}|r| - Y_{|v|r}|v| - Y_{rrr}v^2 - Y_{ur}u \tag{17}$$

$$d_{NL,32}(\boldsymbol{\nu}) = -N_{|v|v}|v| - N_{|r|v}|r| - N_{vvv}v^2 - N_{uv}u \tag{18}$$

$$d_{NL,33}(\boldsymbol{\nu}) = -N_{|r|r}|v| - N_{|v|r}|v| - N_{rrr}r^2 - N_{ur}u, \tag{19}$$

where

$$Y_{ur} = X_{\dot{u}} \tag{20}$$

$$N_{uv} = -(Y_{\dot{v}} - X_{\dot{u}}) \tag{21}$$

$$N_{ur} = Y_{\dot{r}}, \tag{22}$$

which are damping terms which are linearly increasing with the forward speed. These are added to compensate for the Munk moment, and to get a more physically realistic model behavior [2], [8].

III. CONTROL DESIGN

A. Control objective and 4-corner test

The main control objective is to make $\tilde{\boldsymbol{\eta}}(t) \triangleq \boldsymbol{\eta}(t) - \boldsymbol{\eta}_t(t) \to \mathbf{0}$ $t \to \infty$, where $\boldsymbol{\eta}_t(t) = [x_t(t), y_t(t), \psi_t(t)]^\top \in \mathbb{R}^2 \times \mathbb{S}$ represents the pose associated with a target point. The motion of the target is typically defined by a human or generated by a guidance system. For notational simplicity, time t will mostly be omitted for the rest of the paper.

It is desirable to investigate the effect of the magnitude-rate saturation model during different ship maneuvers. For this reason, a 4-corner maneuvering test is used, as shown in Fig. 2. For comparison, the experiments will be conducted with and without using the MRS model to identify notable effects on performance.

The 4-corner maneuvering test is proposed in [9] as a way to compare ship performance of dynamic positioning control algorithms. The ship is first initialized in dynamic positioning to point straight North at heading $0\,(deg)$. Then the following setpoint changes are commanded:

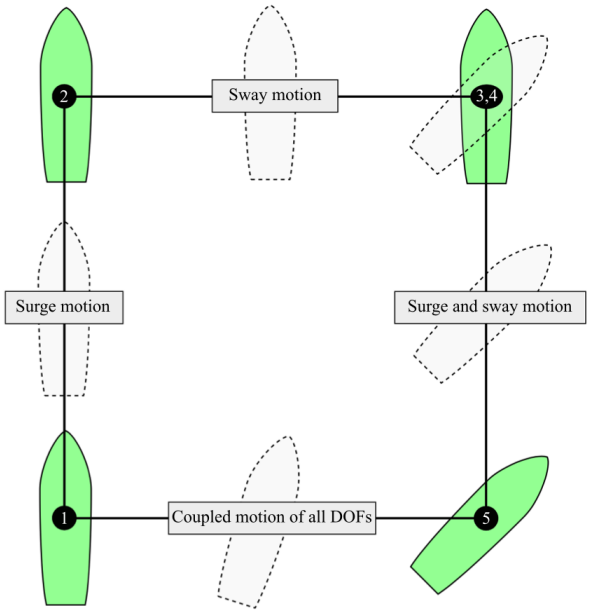

Fig. 2: The 4-corner dynamic positioning test. Modified from [9].

- Position change $2\,(m)$ straight North: tests a pure surge movement ahead.
- Position change $2\,(m)$ straight East: tests a pure sway movement in the starboard direction.
- Heading change $45\,(deg)$ clockwise: tests a pure yaw motion while keeping position steady.
- Position change $2\,(m)$ straight South: tests a combined surge-sway movement while keeping heading steady.
- Position change $2\,(m)$ straight West and heading change $45\,(deg)$ counterclockwise: tests a combined surge-sway-yaw movement.

B. Magnitude-rate saturation model design

Modelling the vessel's actuator constraints is important to ensure that the controller output remains inside a feasible range of values. Both magnitude and rate constraints will impact a vessel's ability to maneuver, and should be handled in the control system.

1) Saturation modeling: A generalized saturation block for an actuator can be modeled as

$$\tau_{s,i}(\tau_i) = \begin{cases} \tau_{i,min} & \text{if } \tau_i \leq \tau_{i,min} \\ \tau_i & \text{if } \tau_{i,min} < \tau_i < \tau_{i,max}, \quad \forall i \in \{1,2,3\}, \\ \tau_{i,max} & \text{if } \tau_i \geq \tau_{i,max} \end{cases} \tag{23}$$

where τ_i is the commanded control input without saturation with $i \in \{1,2,3\}$ to control surge, sway and yaw forces and moment, respectively. The saturation limits are represented by $\boldsymbol{\tau}_{min} = [\tau_{1,min}, \tau_{2,min}, \tau_{3,min}]^\top$ and $\boldsymbol{\tau}_{max} = [\tau_{1,max}, \tau_{2,max}, \tau_{3,max}]^\top$ with negative and positive bounded elements, respectively.

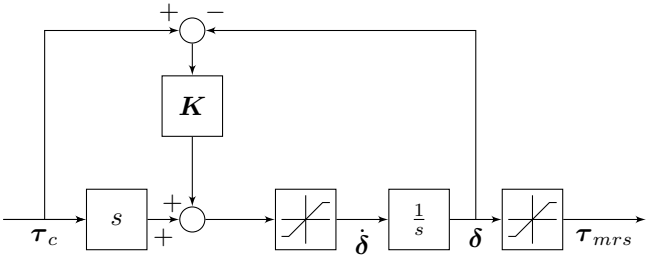

Fig. 3: Block diagram for the MRS model (24).

2) Magnitude-rate saturation model: An approach to model the MRS effects is given by

$$\dot{\boldsymbol{\delta}} = sat_{\boldsymbol{r}}(\dot{\boldsymbol{\tau}}_c + \boldsymbol{K}(\boldsymbol{\tau_c} - \boldsymbol{\delta})) \tag{24}$$

$$\boldsymbol{\tau}_{mrs} = sat_{\boldsymbol{m}}(\boldsymbol{\delta}), \tag{25}$$

where $\boldsymbol{\tau}_c$, $\boldsymbol{\delta}$ and $\boldsymbol{\tau}_{mrs}$ are the input, state and output of the MRS model, respectively, and where $\boldsymbol{K} > 0$ is a diagonal tuning matrix. The matrix is introduced in order to avoid an unstable cancellation between the derivative operator s and the integrator in Fig. 3, where the block diagram for the MRS model is shown. Because of this, an important observation is that neither of the elements of the matrix $\boldsymbol{K}$ can be equal to 1, and thus also $\boldsymbol{K} \neq \boldsymbol{I}$. The gain matrix $\boldsymbol{K}$ affects the speed of the inner-loop in the MRS model, and should be chosen based on the desired tracking performance. The derivative of the input, $\dot{\boldsymbol{\tau}}_c$, is supposed to exist and can be calculated using numerical derivation. The saturation limits $sat_{\boldsymbol{r}}$ and $sat_{\boldsymbol{m}}$ are modeled as the saturation block above, and contain the vessel's rate and magnitude constraints, respectively. See [4] for further details.

In this setup, the rate is limited first and the magnitude next, meaning that the MRS model state $\boldsymbol{\delta}$ can exceed the magnitude-bounds vector $\boldsymbol{m}$, although the output $\boldsymbol{\tau}_{mrs}$ never does. It should also be noted that this model can be further extended to effectively solve anti-windup problems, should such effects be needed to be accounted for.

C. Nonlinear control design

The MRS model will be tested with two types of feedback controllers in order to investigate the impact on performance for both linear and nonlinear feedback terms.

1) Nonlinear pose and linear velocity feedbacks: Using a control scheme based on a combination of nonlinear feedback of pose and linear feedback of velocity from [5], the control input can be chosen as

$$\boldsymbol{\tau} = \boldsymbol{M}\dot{\boldsymbol{\alpha}} + \boldsymbol{C}(\boldsymbol{\nu})\boldsymbol{\alpha} + \boldsymbol{D}(\boldsymbol{\nu})\boldsymbol{\alpha} - \boldsymbol{\Gamma}_2\boldsymbol{z}_2, \tag{26}$$

where

$$\dot{\boldsymbol{\alpha}} = \boldsymbol{R}^\top(\psi)\ddot{\boldsymbol{\eta}}_t + \boldsymbol{S}(r)^\top\boldsymbol{R}^\top(\psi)\dot{\boldsymbol{\eta}}_t - \dot{\boldsymbol{K}}_1(\cdot)\boldsymbol{z}_1 - \boldsymbol{K}_1(\cdot)\dot{\boldsymbol{z}}_1, \tag{27}$$

with $\boldsymbol{\Gamma}_2 > 0$ and where

$$\boldsymbol{S}(r) = \begin{bmatrix} 0 & -r & 0 \\ r & 0 & 0 \\ 0 & 0 & 0 \end{bmatrix}. \tag{28}$$

Here, the error variables $\boldsymbol{z}_1 = [z_{1,x}, z_{1,y}, z_{1,\psi}]^\top$ and $\boldsymbol{z}_2 = [z_{2,u}, z_{2,v}, z_{2,r}]^\top$ are defined as

$$\boldsymbol{z}_1 \triangleq \boldsymbol{R}(\psi)(\boldsymbol{\eta} - \boldsymbol{\eta}_t) \tag{29}$$

$$\boldsymbol{z}_2 \triangleq \boldsymbol{\nu} - \boldsymbol{\alpha}, \tag{30}$$

where $\boldsymbol{\alpha} \in \mathbb{R}^3$ is a vector of stabilizing functions, which can be interpreted as a desired velocity. As in [5], $\boldsymbol{\alpha}$ can be chosen as

$$\boldsymbol{\alpha} = \boldsymbol{R}^\top(\psi)\dot{\boldsymbol{\eta}}_{\boldsymbol{t}} - \boldsymbol{K}_1(\cdot)\boldsymbol{z}_1, \tag{31}$$

with the nonlinear feedback term $\boldsymbol{K}_1(\cdot)$ chosen as

$$\boldsymbol{K_1}(\cdot) = \boldsymbol{\Gamma}_1 \begin{bmatrix} \dfrac{1}{\sqrt{\boldsymbol{z}_{1,\tilde{p}}^\top \boldsymbol{z}_{1,\tilde{p}} + \Delta_{\tilde{p}}^2}} \boldsymbol{I}_{2\times 2} & \boldsymbol{0}_{2\times 1} \\ \boldsymbol{0}_{1\times 2} & \dfrac{1}{\sqrt{z_{1,\tilde{\psi}}^2 + \Delta_{\tilde{\psi}}^2}} \end{bmatrix}, \tag{32}$$

where $\boldsymbol{z}_{1,\tilde{p}} = [z_{1,x}, z_{1,y}]^\top$, $\boldsymbol{\Gamma}_1 > 0$ and $\Delta_i > 0$ are tuning parameters. Furthermore, $\dot{\boldsymbol{K}}_1(\cdot)$ is given by

$$\dot{\boldsymbol{K}}_1(\cdot) = -\boldsymbol{\Gamma}_1 \begin{bmatrix} \dfrac{\boldsymbol{z}_{1,\tilde{p}}^\top \dot{\boldsymbol{z}}_{1,\tilde{p}}}{(\boldsymbol{z}_{1,\tilde{p}}^\top \boldsymbol{z}_{1,\tilde{p}} + \Delta_{\tilde{p}}^2)^{\frac{3}{2}}} \boldsymbol{I}_{2\times 2} & \boldsymbol{0}_{2\times 1} \\ \boldsymbol{0}_{1\times 2} & \dfrac{z_{1,\tilde{\psi}}\dot{z}_{1,\tilde{\psi}}}{(z_{1,\tilde{\psi}}^2 + \Delta_{\tilde{\psi}}^2)^{\frac{3}{2}}} \end{bmatrix}. \tag{33}$$

2) Nonlinear pose and velocity feedbacks: The other control scheme from [5] augments (26) with a nonlinear velocity feedback term, giving the control input

$$\boldsymbol{\tau} = \boldsymbol{M}\dot{\boldsymbol{\alpha}} + \boldsymbol{C}(\boldsymbol{\nu})\boldsymbol{\alpha} + \boldsymbol{D}(\boldsymbol{\nu})\boldsymbol{\alpha} - \boldsymbol{K}_2(\cdot)\boldsymbol{z}_2, \tag{34}$$

where $\dot{\boldsymbol{\alpha}}$ and $\boldsymbol{\alpha}$ are given by (27) and (31), respectively, and with the nonlinear feedback term $\boldsymbol{K}_2(\cdot)$ chosen as

$$\boldsymbol{K_2}(\cdot) = \boldsymbol{\Gamma}_2 \begin{bmatrix} \dfrac{1}{\sqrt{\boldsymbol{z}_{2,\tilde{\nu}^\top} \boldsymbol{z}_{2,\tilde{v}} + \Delta_{\tilde{v}}^2}} \boldsymbol{I}_{2\times 2} & \boldsymbol{0}_{2\times 1} \\ \boldsymbol{0}_{1\times 2} & \dfrac{1}{\sqrt{z_{2,\tilde{r}^2} + \Delta_{\tilde{r}}^2}} \end{bmatrix}, \tag{35}$$

where $\boldsymbol{z}_{2,\tilde{v}} = [z_{2,u}, z_{2,v}]^\top$ and $\Delta_i > 0$ are tuning parameters. The feedback gain $\boldsymbol{\Gamma}_2$ is the same matrix as in (26).

The nonlinear pose and linear velocity feedback controller and the nonlinear pose and velocity feedback controller will be abbreviated NP-LV and NP-NV, respectively, throughout the rest of this paper.

TABLE II: Control gains.

	NP-LV	**NP-NV**
$\boldsymbol{\Gamma}_1$	$\text{diag}([0.08, 0.08, 0.0698])$	$-\|\|-$
$\boldsymbol{\Gamma}_2$	$\text{diag}([0.2, 0.2, 0.1745])\boldsymbol{M}$	$-\|\|-$
$\Delta_{\tilde{p}}$	0.5	$-\|\|-$
$\Delta_{\tilde{\psi}}$	0.5	$-\|\|-$
$\Delta_{\tilde{v}}$	$-$	0.7
$\Delta_{\tilde{r}}$	$-$	1
$\boldsymbol{K}$	$\text{diag}([4, 3, 2])$	$-\|\|-$

3) Stability: Based on the theorems and stability proofs in [10], we can conclude that the two controllers have the following stability properties: The origin $(\boldsymbol{z}_1, \boldsymbol{z}_2) = (\boldsymbol{0}, \boldsymbol{0})$ is uniformly globally asymptotically stable (UGAS) and on each compact set $B \subset \mathbb{R}^6$ containing the origin, it is uniformly exponentially stable (UES) [10]. The MRS model is a nonlinear filter, and it is proven in [4] that the output will be an $\mathcal{L}_2$ signal if the input is an $\mathcal{L}_2$ signal, so it can be concluded that the MRS model does not alter the stability properties of the system.

4) Parameter tuning: The experiments are conducted with the gain parameters shown in Table II. The choice of the gain parameters for the two controllers are based on the tuning rules described in [10]. Here, the goal is to make the kinetic subsystem faster than the kinematic subsystem, which means that the kinetic subsystem needs to have smaller time constants than the kinematic subsystem in the linear region. The Δ-values scale the linear feedback gains and therefore the resulting time constants of the linear region, and must therefore be chosen such that they do not make the kinematic subsystem faster than the kinetic subsystem.

The actuator saturation limits are chosen by the following set of suggested tuning rules as well [11]. Here, the magnitude saturation limits are set lower than the actual limitations in order to save energy, and chosen as $\boldsymbol{m} = [2, 1.5, 1]$. The rate saturation limits are chosen by $\boldsymbol{r} = [m_1/t_{mrs,1}, m_2/t_{mrs,2}, m_3/t_{mrs,3}]^\top$, where m_1, m_2 and m_3 are the magnitude saturation limits given by $\boldsymbol{m}$, and where $t_{mrs,1}$, $t_{mrs,2}$ and $t_{mrs,3}$ are the desired transition times for the actuators to go from zero to max thrust in surge, sway and yaw, respectively. Here, suitable values for the rate saturation limits were found to be $\boldsymbol{r} = [1.9, 1.1, 0.8]$. Then, the gain matrix $\boldsymbol{K}$ can be chosen by $\boldsymbol{K} = \text{diag}([K_{1,1}, \frac{m_2}{m_1}K_{1,1}, \frac{m_3}{m_1}K_{1,1}])$, where under normal operations it is desired to have all the diagonal elements $\boldsymbol{K}_{i,i} > 1$, $\forall i \in \{1, 2, 3\}$. Here, $K_{1,1} = 4$ to ensure a fast tracking of the target signal in all three degrees of freedom. The block diagram for the full control system is shown in Fig. 4.

IV. EXPERIMENTAL RESULTS AND PERFORMANCE EVALUATION

A. Marine Cybernetics Laboratory

As already mentioned, the MC-Lab is a small ocean basin at NTNU. Due to its relatively small size and advanced instrumentation package, the facility is especially suited for

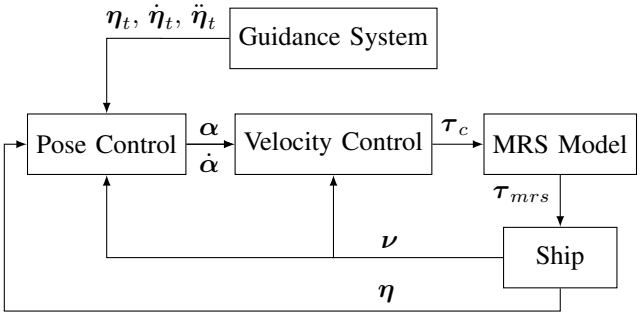

Fig. 4: Block diagram for the ship control system.

tests of motion control systems for marine vessel models, but is also suitable for more specialized hydrodynamic tests due to the advanced towing carriage, which has capability for precise movement of models up to six degrees of freedom [12].

The experiments will be conducted under the following conditions: In the experiments, the actual model ship's $\boldsymbol{M}$, $\boldsymbol{C}$ and $\boldsymbol{D}$ matrices will differ somewhat from those used in the controllers. Also, measurement noise is present in the Qualisys motion tracking system used in the laboratory.

B. Performance metrics

Performance metrics are used to objectively compare the performance of different control schemes. In this paper, the error variable is defined as the scaled norm of the pose control error $\boldsymbol{z}_1$, such that

$$e = \sqrt{\bar{\boldsymbol{z}}_1^\top \bar{\boldsymbol{z}}_1}, \tag{36}$$

where

$$\bar{\boldsymbol{z}}_1 = [\frac{z_{1,x}}{4}, \frac{z_{1,y}}{4}, \frac{z_{1,\psi}}{\pi/2}]^\top. \tag{37}$$

Since the position and yaw angle in pose have different units, we have defined the normalized pose error signals $\bar{z}_{1,x}$, $\bar{z}_{1,y}$ and $\bar{z}_{1,\psi}$ on the intervals $[-0.5, 0.5]$ in the expected operational space of the ship [13]. To get this interval, the position errors are divided by 4 and the yaw error is divided by $\frac{\pi}{2}$, since the position errors are in the intervals $[-2, 2]$ and the yaw error is in the interval $[-\frac{\pi}{4}, \frac{\pi}{4}]$, resulting in the normalized control error e.

Three different performance metrics are used in this paper, namely IAE, IAEW and IADC. The IAE (integral of the absolute error) metric is defined as an unweighted integral over time:

$$IAE(t) = \int_0^t |e(\gamma)|\, d\gamma. \tag{38}$$

The IAEW (integral of the absolute error multiplied by energy consumption) metric scales IAE by the energy consumption

$$IAEW(t) = \int_0^t |e(\gamma)|\, d\gamma \int_0^t P(\gamma) d\gamma, \tag{39}$$

where $P = \left|\boldsymbol{\nu}^\top \boldsymbol{\tau}\right|$, thus yielding a measure of energy efficiency.

Since the aim of the MRS model is also to reduce actuator wear and tear, it is interesting to investigate the dynamic behavior of the control signal. The IADC (integral of absolute differentiated control) metric is defined as in [13]:

$$IADC(t) = \int_{t_0}^t |\dot{\bar{\tau}}(\gamma)|\, d\gamma, \tag{40}$$

with $\bar{\tau}(t) = \sqrt{\boldsymbol{\tau}^\top \boldsymbol{\tau}}$, and where $\dot{\bar{\tau}}$ is computed using numerical derivation.

C. Experimental results

In the experiments, the target pose changes between setpoints for the 4-corner test. The system is implemented such that the target will automatically change to the next setpoint when the ship is within 0.003 m from the target in both x and y direction and 0.2 deg from the target heading. When the 4-corner test is completed, the ship will have returned accurately to its initial position and heading, ready for a new test at the same pose and along the same track.

While CSAD has a length of $L = 2.578$ m, its outline has been scaled by 1:6 in the 4-corner plots in Fig. 5 and 8, to better display the ship behaviour. By the plotted values of the performance metrics in Fig. 6 and 9, the effects of the MRS model on control performance can be examined. Fig. 5 shows the 4-corner track and the actual trajectory for the CSAD with and without the MRS model applied to the NP-LV controller. The results show no remarkable difference in the trajectory.

The performance metrics are plotted in Fig. 6. The metrics show that the while MRS does not reduce the overall tracking error by the IAE metric, both energy consumption (IAEW) and actuator wear and tear (IADC) are reduced by 6.8% and 38.8%, respectively.

In Fig. 7, the commanded thrust signals are shown for the 4-corner test. It can be seen that the MRS contributes to a smoother and amplitude-wise smaller control signal, while achieving approximately the same tracking performance. The spikes that can be seen in the control signal, especially during transients, are caused by noise related to the velocity estimation.

Fig. 8 displays the 4-corner trajectory for the NP-NV controller. Even though the NP-NV-controlled vessel with MRS effects takes a wider arch in the coupled motion ($5 \rightarrow 1$) in Fig. 2, the overall tracking error is not increased, as seen in Table III.

Furthermore, Fig. 9 shows improvement in energy efficiency, shown by the IAEW metric, and lower actuator wear and tear through the IADC metric. The reduction is greater for the NP-NV controller than the NP-LV controller, which is due to the fact the NP-NV is inherently a more aggressive controller, and thus benefits more from using an MRS model. For the NP-NV controller, the reduction is 12.2% and 46.4% for IAEW and IADC, respectively.

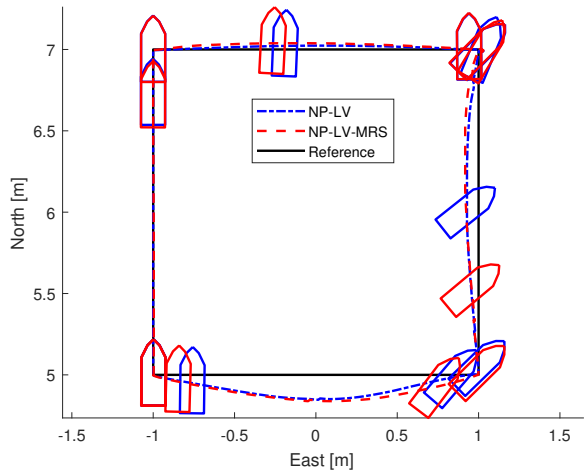

Fig. 5: Vessel performing the 4-corner manoeuver using the NP-LV controller.

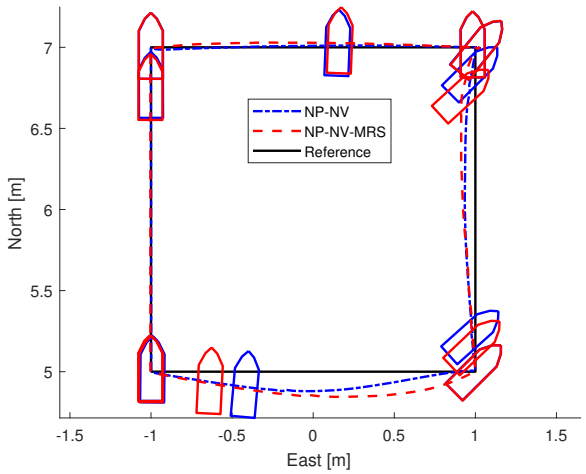

Fig. 8: Vessel performing the 4-corner maneuver using the NP-NV controller.

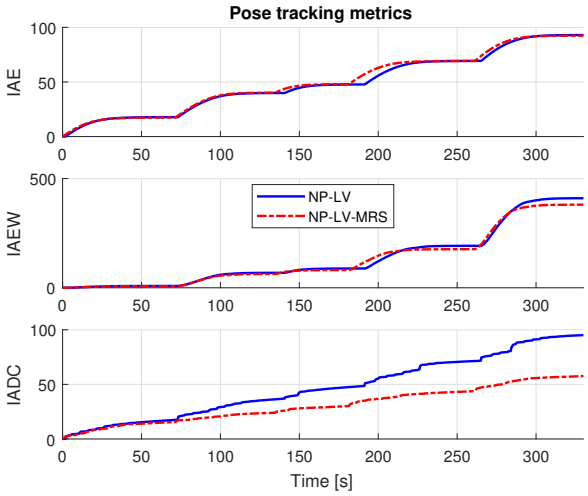

Fig. 6: Performance metrics for NP-LV.

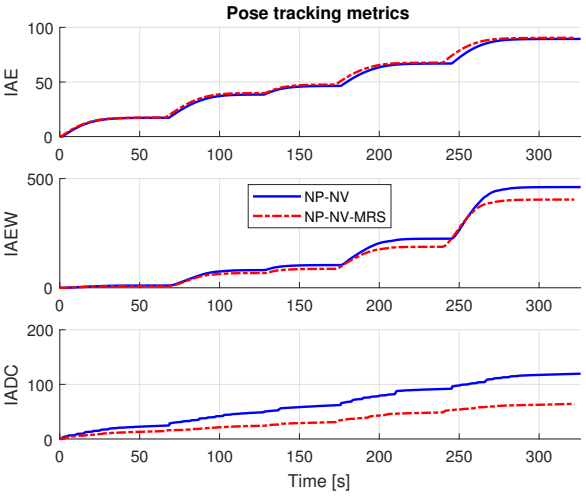

Fig. 9: Performance metrics for NP-NV.

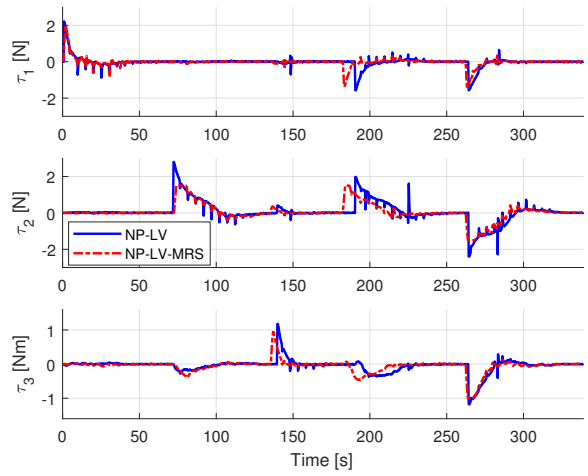

Fig. 7: Commanded control input for NP-LV.

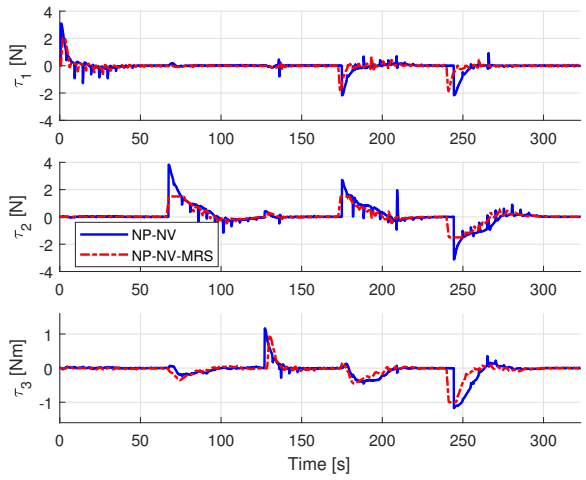

Fig. 10: Commanded control input for NP-NV.

TABLE III: Performance metrics final values.

	NP-LV	NP-LV MRS	NP-NV	NP-NV MRS
IAE final	92.99	**92.85**	**89.49**	90.38
IAEW final	410.12	**382.23**	460.08	**403.79**
IADC final	95.99	**58.73**	118.26	**63.34**

Fig. 10 shows the commanded control inputs for the NP-NV controller. Similar to NP-LV, a smoothing effect can be observed, although less significant. This is likely due to the nature of the pure nonlinear feedback, giving overall better tracking performance, which has previously been discussed in [5].

A significant effect of the MRS model, which can be seen in the performance metrics in Fig. 6 and 9, is that it results in a significantly reduced rate of change in the commanded control input.

The final values for the performance metrics are displayed in Table III, where the best performing controller for the different metrics is noted in bold.

V. CONCLUSION

Depending on the type of controller that is being used, including an MRS model to limit the actuator magnitude and rate outputs can contribute positively in several ways. As seen in both cases presented, an MRS model can effectively reduce actuator twitching, and thus wear and tear, without the degradation of performance in ship control. In addition, it has the potential to improve overall energy efficiency and pose tracking abilities, as can be seen from the performance metrics and trajectory plots, and can thus have positive effects on ship performance in setpoint navigation. These effects are especially important for vessels which must operate for long times at sea, and can be particularly useful for ships in DP operations, effectively contributing to the longevity of the operation with a reduced need for maintenance and repairs.

Future work includes optimizing the MRS model to further improve performance. This includes, through experimental tests in a laboratory, further tuning of the gain matrix $\boldsymbol{K}$ and the desired magnitude and rate saturation effects to obtain optimal ship control for the wanted ship operational environment.

ACKNOWLEDGEMENTS

This work was supported by the Research Council of Norway through the Centres of Excellence funding scheme, project number 223254. The authors gratefully acknowledge senior engineer Torgeir Wahl and Ph.D. candidate Andreas R. Dahl at NTNU's Department of Marine Technology for valuable support during the experiments.

REFERENCES

[1] V. Kapila and S. Valluri, "Model predictive control of systems with actuator amplitude and rate saturation," *in Proceedings of the 37th IEEE Conference on Decision and Control, pp. 1396-1401*, 1998.

[2] M. E. N. Sørensen, M. Breivik, and B.-O. H. Eriksen, "A ship heading and speed control concept inherently satisfying actuator constraints," *in Proceedings of the 1st IEEE Conference on Control Technology and Applications, HI, USA*, 2017.

[3] M. E. N. Sørensen, O. N. Lyngstadaas, B.-O. H. Eriksen, and M. Breivik, "A dynamic window-based controller for dynamic positioning satisfying actuator magnitude constraints," *in Proceedings of the 11th IFAC Conference on Control Applications in Marine Systems, Robotics, and Vehicles, Opatija, Croatia*, 2018.

[4] S. Galeani, S. Onori, A. R. Teel, and L. Zaccarian, "A magnitude and rate saturation model and its use in the soluton of a static anti-windup problem," *Systems & Control Letters, Volume 57, Issue 1, pp. 1-9*, 2008.

[5] M. E. N. Sørensen and M. Breivik, "Comparing combinations of linear and nonlinear feedback terms for motion control of marine surface vessels," *in Proceedings of the 10th IFAC Conference on Control Applications in Marine Systems, Trondheim, Norway*, 2016.

[6] T. I. Fossen, *Handbook of Marine Craft Hydrodynamics and Motion Control*. Wiley, 2011.

[7] J. Bjørnø, *Thruster-Assisted Position Mooring of C/S Inocean Cat I Drillship*. Master thesis, Norwegian University of Science and Technology, Trondheim, Norway, 2016.

[8] J. E. Refsnes, *Nonlinear Model-Based Control of Slender Body AUVs*. PhD thesis, Norwegian University of Science and Technology, Trondheim, Norway, 2008.

[9] R. Skjetne, M. E. N. Sørensen, M. Breivik, S. A. T. Værnø, A. H. Brodtkorb, A. J. Sørensen, Ø. K. Kjerstad, V. Calabrò, and B. O. Vinje, "AMOS DP research cruise 2016: Academic full-scale testing of experimental dynamic positioning control algorithms onboard R/V Gunnerus," *in Proceedings of the 36th International Conference on Ocean, Offshore and Arctic Engineering*, 2017.

[10] M. E. N. Sørensen, M. Breivik, and R. Skjetne, "Comparing combinations of linear and nonlinear feedback terms for ship motion control," *submitted to IEEE Transactions on Control Systems Technology*, 2018.

[11] O. N. Lyngstadaas, *Ship Motion Control Concepts Considering Actuator Constraints*. Master thesis, Norwegian University of Science and Technology, Trondheim, Norway, 2018.

[12] "Marine cybernetics laboratory." https://www.ntnu.edu/imt/lab/cybernetics. Accessed: 2018-01-30.

[13] B.-O. H. Eriksen and M. Breivik, *Modeling, Identification and Control of High-Speed ASVs: Theory and Experiments*, pp. 407–431. Sensing and Control for Autonomous Vehicles: Applications to Land, Water and Air Vehicles, Springer International Publishing, 2017.